Electrochimica Acta 253 (2017) 257–267

Contents lists available at ScienceDirect

Electrochimica Acta

journal homepage: www.elsevier.com/locate/electacta

Research Paper

The effect of chloride ions on the electrochemical dissolution of chalcopyrite in sulfuric acid solutions

Qingyou Liu[a,*], Miao Chen[b], Yi Yang[b]

[a] Institute of Geochemistry, Chinese Academy of Sciences, Guiyang 550002, China
[b] CSIRO Mineral Flagship, Clayton, Victoria, 3169, Australia

ARTICLE INFO

Article history:
Received 26 March 2017
Received in revised form 13 June 2017
Accepted 12 September 2017
Available online 14 September 2017

Keywords:
chalcopyrite
chloride ions
potentiodynamic curve
cyclic voltammetry
EIS
electrochemical dissolution

ABSTRACT

The dissolution of chalcopyrite in 0.2 M sulfuric acid solutions with different sodium chloride concentrations was investigated. Different anodic potentials were applied, and the behavior of the electrode was observed using potentiodynamic, cyclic voltammetry (CV), and electrochemical impedance spectroscopy (EIS) techniques. The results showed that the chalcopyrite open circuit potential (OCP, approximately 245 mV vs. SCE) decreased as the NaCl concentration increased. Four different surface conditions emerged on the chalcopyrite surface as the anodic potentials increased: (1) a $Cu_{1-x}Fe_{1-y}S_2$ passive layer formed at OCP–500 mV; (2) a second passive layer ($Cu_{1-x-z}S_2$) formed at 500–700 mV (electrolyte without NaCl) or 500–800 mV (electrolyte with NaCl); and (3) chalcopyrite was in an active area at 700–800 mV (electrolyte without NaCl) or 800–900 mV (electrolyte with NaCl), and all the previous passive layers disappeared. In this case, SO_4^{2-} or $S_2O_3^{2-}$ and $S_4O_6^{2-}$ for the electrolyte without NaCl or with NaCl, respectively, are the oxidized forms of sulfide sulfur; (4) when the potential is above 800 mV (for the electrolyte without NaCl) or 900 mV (for the electrolyte with NaCl), pseudo-passive CuS is formed. Subsequently, the sulfur of CuS was oxidized to SO_4^{2-}, and Cu^{2+} changed into $CuCl^+$ with a NaCl concentration of 0 mol/L and 0.5 mol/L, respectively. However, a new passive layer(s) of $Cu_2(OH)_3Cl$ formed with NaCl concentrations above 0.5 mol/L. Overall, the results revealed that Cl^- ions are advantageous for chalcopyrite dissolution. However, the oxidation of chalcopyrite generated chloride and cupric ions that can form the cuprous complexes $CuCl^0$, $CuCl_2^-$ or $CuCl_3^{2-}$, which dramatically inhibit the on-going dissolution of chalcopyrite. EIS data confirmed that a high concentration of Cl^- ions was not essential for chalcopyrite dissolution under the present conditions. Moreover, the critical Cl^- ion concentrations were different for the four distinct potential areas outlined above, namely, 1.0 mol/L, 1.25 mol/L, 1.25 mol/L and 0.5 mol/L, respectively.

1. Introduction

Chalcopyrite ($CuFeS_2$), one of the most abundant primary copper ores, is mined extensively for its copper, with the extractive method changing from traditional thermometallurgy to hydrometallurgy. Nicol [1] indicated that the interest in the electrochemistry of sulfide minerals stems largely from the fact that their dissolution in oxidizing solutions occurs via an electrochemical mechanism. This mechanism is important in hydrometallurgical processes and in the surface activation of sulfide minerals prior to flotation [2]. Therefore, many reports have emerged to clarify the dissolution kinetics of chalcopyrite in different media using various electrochemical techniques [3–7].

Because of its strong oxidation-reduction quality and complex power, chloride ions have always been employed in electrochemical studies of sulfide minerals. For example, Ammou-Chokroum et al. [8,9] investigated the anodic behavior of chalcopyrite in chloride media, with a particular emphasis on the dissolution of chalcopyrite in acidic solutions. They postulated that the initial stage of dissolution involves the formation of hydrogen sulfide, ferrous ions and covellite. Furthermore, they postulated that the ohmic potential drop across the precipitated chalcocite plays an important role in establishing the electrochemical behavior of chalcopyrite. McMillan et al. [10] studied the anodic dissolution of chalcopyrite in both acidic sulfate and acidic chloride media and suggested that the slow the rate of electron transfer is caused by the formation of a surface layer. In the hydrometallurgical field,

* Corresponding author.
E-mail address: liuqingyou@vip.gyig.ac.cn (Q. Liu).

http://dx.doi.org/10.1016/j.electacta.2017.09.063
0013-4686/

chlorides have always been used for the hydrometallurgical treatment of sulfide ores, particularly complex sulfides, because of their high degree of leaching power efficiency [11–14]. Researchers have reported that the cause of this fast leaching rate in chloride is morphological, whereby a porous coating layer is formed on the chalcopyrite particles during the leaching process in the chloride medium [15,16]. The role of chloride ions is believed to limit the extent of passivation by elemental sulfur [17,18]. Note that increases in the chloride concentration had little effect on the leaching rate of chalcopyrite with chloride concentrations above 0.5 mol/L [15,19].

In this work, the electrochemical dissolution of chalcopyrite in sulfuric acid solutions with different chloride ion concentrations was studied. First, the potentiodynamic curve was used to understand the chalcopyrite electrode passivation, trans-passivation and activation potential intervals. Cyclic voltammetry (CV) was then used to acquire qualitative information on the electrochemical reactions. Finally, electrochemical impedance spectroscopy (EIS) experiments were performed to study the electrode characteristics and the electrochemical reactions at different potential intervals. The aim of this work was to determine how the chloride ions affect the surface properties and growth sequence of chalcopyrite surface layers in a sulfuric acid solution at different anodic potentials. This work also seeks to provide an experimental basis for the highly effective electrochemical leaching of chalcopyrite in the presence of chloride ions conditions.

2. Experimental

2.1. Electrode preparation

High quality natural polycrystalline chalcopyrite was obtained from Mt Lyell, Australia. X-ray diffraction analysis confirmed that the Fe, Cu and S contents (wt %) of chalcopyrite were 30.8%, 33.7% and 34.2%, respectively. Chalcopyrite electrodes were prepared by cutting the chalcopyrite samples into approximately cube-like shapes with working areas of 0.25 cm^2, and as much as possible, with no visible imperfections. The specimens were placed on an epoxy resin and connected to a copper wire by silver paint on the back face, leaving only one face of the electrode exposed to the solution. Prior to each test, the chalcopyrite electrode was polished with no. 1200 carbide paper to obtain fresh surfaces, and then degreased by alcohol. The electrode was then rinsed with deionized water and dried in a stream of air.

2.2. Electrochemical measurements

Electrochemical measurements were performed using a computer-controlled electrochemical measurement system (PARSTAT 2273, Princeton Applied Research) on a conventional three-electrode electrolytic cell with platinum as an auxiliary electrode (AE) and chalcopyrite as the working electrode (WE). A saturated calomel electrode (SCE) was used as the reference electrode for all of the electrochemical tests; unless otherwise mentioned, all further potentials reported in this study are relative to the SCE (0.242 V vs. standard hydrogen electrode). The reference electrode was connected to a Luggin capillary to minimize the resistance of the solution between the working and reference electrodes. The electrolyte was composed of 0.2 mol/L H_2SO_4 with different NaCl concentrations: (1) 0 mol/L, (2) 0.5 mol/L, (3)1.0 mol/L, (4) 1.25 mol/L and (5) 1.5 mol/L. The working, auxiliary and reference electrodes were each situated in the same position to ensure identical spatial relationships for each experiment. All of the experiments were conducted at 25 ± 1 °C.

Potentiodynamic curves, CV and EIS were utilized to study the behaviors of the chalcopyrite electrode. First, the chalcopyrite electrodes open circuit potential (OCP) was measured, and the electrochemical experiments started only when the OCP reached a quasi-steady state. In this study, potentiodynamic cycles were performed with a positive-going potential sweep from OCP to + 0.8 V/1.0 V (0.8 V is the electrolyte without NaCl and 1.0 V is the electrolyte with NaCl) and back with a negative-going potential sweep from + 0.8 V/1.0 V to − 0.60 V, and then a positive-going potential sweep back to + 0.8 V/1.0 V at a scan rate of 5 mV s^{-1}. Potentiodynamic polarization curves were obtained by automatically changing the electrode potential from −100 mV to 1000 mV at a scan rate of 0.5 mV s^{-1}. EIS tests were conducted at different potentials in the frequency range of 0.01 ~ 10000 Hz with a peak-to-peak amplitude of 10 mV. The electrode potential was allowed to stabilize for 400 s before commencement of the measurements. ZSimpWin 3.20 (2004) software was used to fit the impedance data.

3. Results and discussion

3.1. Open circuit potential study

The open circuit potential curves of the chalcopyrite electrode in 0.2 mol/L sulfuric acid solutions with different NaCl concentrations (0, 0.5, 1.0, 1.25 and 1.5 mol/L) as a function of time are shown in Fig. 1. As seen, sodium chloride causes a decrease in the chalcopyrite OCP as the NaCl concentration increases. Furthermore, the electrode potential increases for 10 min before reaching a quasi-steady state in all of the curves, which indicates the spontaneous growth of a passive film on the electrode surface. The steady state OC potentials were found to be approximately 245 ± 10 mV, 122 ± 10 mV, 108 ± 10 mV, 95 ± 10 mV and 84 ± 10 mV, respectively, where the steady-state was defined here as a change of less than 2 mV/min.

Antonijević et al. [20] indicated that the chalcopyrite potential in redox solutions could be defined as: $E_{CuFeS_2} = E_{const} + n\log[Ox]/[Red]$, where E_{CuFeS_2} is the chalcopyrite potential, V; E_{const} is the chalcopyrite potential when [Ox] = [Red], V; n is the slope of line in the system $E_{CuFeS_2} = f(\log [Ox]/[Red])$; [Ox] is the concentration of oxidized species, M; and [Red] is the concentration of reduced species, mol/L.

As mentioned above, sodium chloride causes the chalcopyrite OCP to decrease as the NaCl concentration increases. One reason for this phenomenon is related to the amount of oxygen present in the solution. The presence of chloride ions in solution reduces the

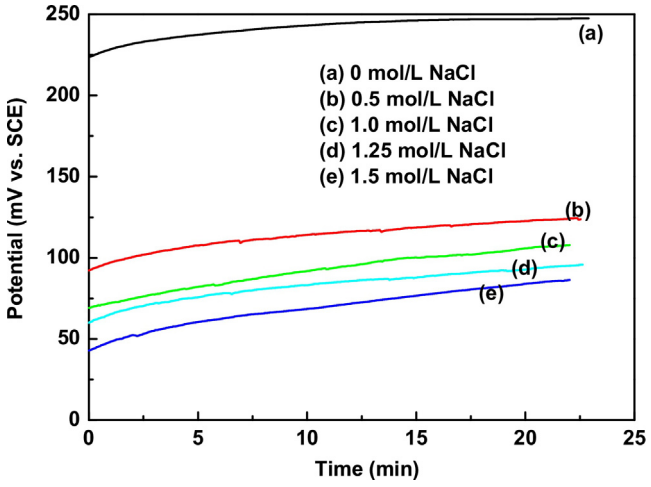

Fig. 1. Time-potential relationships of chalcopyrite in 0.2 mol/L sulfuric acid with different NaCl concentrations.

amount of available oxygen [21], resulting in a smaller [Ox]. A second, and possibly more fundamental reason for this behavior, is the fact that chalcopyrite reaches an electrochemical quasi-steady state, which can be described by the normal mixed-potential electrochemical model proposed by Jones and Peters [22] and Miller et al. [23] shown in Reaction (1). When the electrolyte contained Cl^-, Lin et al. [24] and Lundström et al. [25] reported that Cl^- and Cu^{2+} form a series of chloro-complexes such $CuCl^0$, $CuCl_2^-$ or $CuCl_3^{2-}$, as shown in Reactions (2)–(4). The formation of these cuprous chloride complexes disturbs the balance of chalcopyrite and Cu^{2+} ions, and restoring this balance causes the chalcopyrite to release more Cu^{2+} ions; that is, a larger [Red] value develops, causing the chalcopyrite OCP to decrease.

$$CuFeS_2 \rightarrow Cu^{2+} + Fe^{3+} + 2S^0 + 5e^- \quad (1)$$

$$Cu^{2+} + Cl^- + e^- = CuCl^0 \quad 0.558\,V \quad (2)$$

$$Cu^{2+} + 2Cl^- + e^- = CuCl_2^- \quad 0.470\,V \quad (3)$$

$$Cu^{2+} + 3Cl^- + e^- = CuCl_3^{2-} \quad 0.494\,V \quad (4)$$

3.2. Potentiodynamic study

Potentiodynamic curves for the chalcopyrite electrode in 0.2 mol/L sulfuric acid solutions with different NaCl concentrations (0, 0.5, 1.0, 1.25 and 1.5 mol/L) at a scan rate of 0.5 mV s^{-1} are shown in Fig. 2.

The potentiodynamic *E-i* profile showed a similar result to that reported by Ghahremaninezhad et al. [26] for the electrolyte without NaCl during the anodic scan. For the electrolyte with NaCl, the potentiodynamic curves show similar *E-i* profiles to those without NaCl, suggesting that two sample surfaces have similar initial properties and identical electrochemical interaction mechanisms. Regardless of whether the electrolyte contained NaCl, the potentiodynamic curves showed a clear passive area from the OCP to approximately 500 mV at low anodic potentials, which is consistent with the formation of a thin $Cu_{1-x}Fe_{1-y}S_2$ surface layer via Reactions (5) and (6), as reported by Hackl et al. [27].

$$CuFeS_2 + 4H_2O \rightarrow Cu_{1-x}Fe_{1-y}S_2 + xCu^{2+} + yFe^{3+} + zSO_4^{2-} + 8zH^+ + (2\times + 3y + 6z)\,e^- \quad (5)$$

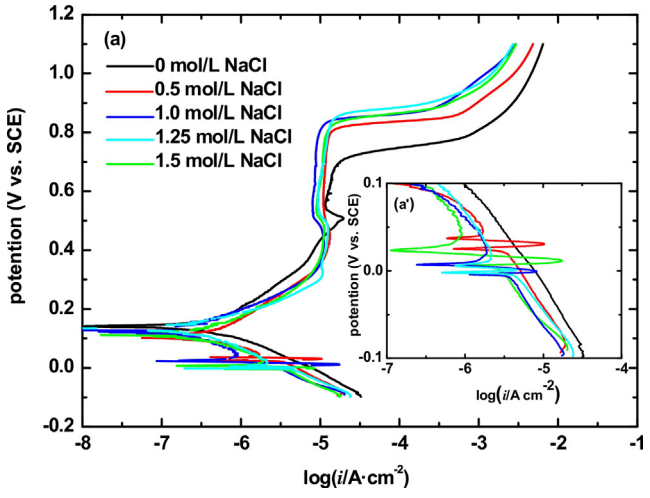

Fig. 2. Potentiodynamic curves for the chalcopyrite electrode in 0.2 mol/L sulfuric acid with different NaCl concentrations at a scan rate 0.5 mV S^{-1}.

or $CuFeS_2 \rightarrow Cu_{1-x}Fe_{1-y}S_2 + xCu^{2+} + yFe^{2+} + 2(x+y)\,e^- \quad y \gg x$ (6)

For the electrolyte without NaCl, a trans-passive dissolution and passive area occurs at potential values of 500–700 mV. According to Parker et al. [28], the previous surface layer $Cu_{1-x}Fe_{1-y}S_2$ transforms into a $Cu_{1-x-z}S_2$ surface layer via Reaction (7). When the electrolyte contains NaCl, chalcopyrite has a broader trans-passive dissolution and passive area at 500–800 mV. These changes are attributed to the formation of $CuCl^0$, $CuCl_2^-$ or $CuCl_3^{2-}$, as mentioned above. These cuprous chloride complexes, especially $CuCl_2^-$ and $CuCl_3^{2-}$, can adsorb easily on the chalcopyrite anodic electrode surface, causing chalcopyrite electrochemical polarization. Clearly, these complexes also inhibited the dissolution of the surface film.

$$Cu_{1-x}Fe_{1-y}S_2 \rightarrow Cu_{1-x-z}S_2 + zCu^{2+} + (1-y)Fe^{2+} + 2(z+1-y)\,e^- \quad (7)$$

As the anodic potential reaches 700 mV for the electrolyte without NaCl, all the surface layer(s) dissolve and the electrodes enter an active area. Biegler [29], Hackl et al. [27] and Lazaro and Nicol [30] demonstrated that the most probable reactions that occur in this region are Reactions (8) and (9), and SO_4^{2-} ions are the most probable oxidized form of sulfide sulfur. However, if the electrolyte contains NaCl, then the chalcopyrite active potential is greater than 800 mV, and the most probable oxidized form of sulfide sulfur is $S_2O_3^{2-}$, as shown in Reaction (10) and reported by Lazaro and Nicol [30]. Furthermore, when the anodic potential was greater than 850 mV, Lehmann et al. [31] and Antonijević et al. [32] reported that $S_2O_3^{2-}$ became $S_4O_6^{2-}$ via Reaction (11). These distinct oxidation mechanisms will be explored using CV and EIS. Regardless of the uncertainty concerning the sulfide sulfur oxidation mechanisms, the consensus is that sulfur is transformed sequentially to sulfates at potentials over the trans-passive region.

$$Cu_{1-x-z}S_2 \rightarrow (1\text{-}x\text{-}z)Cu^{2+} + 2S^0 + 2(1\text{-}x\text{-}z)e^- \quad (8)$$

$$CuFeS_2 + 8H_2O \rightarrow Cu^{2+} + Fe^{3+} + 2SO_4^{2-} + 16H^+ + 17e^- \quad (9)$$

$$CuFeS_2 + 3H_2O \rightarrow Cu^{2+} + Fe^{2+} + S_2O_3^{2-} + 6H^+ + 8e^- \quad (10)$$

$$2S_2O_3^{2-} = S_4O_6^{2-} + 2e^- \quad (11)$$

As the anodic potential continues to increase above 800 mV (for the electrolyte without NaCl) or 900 mV (for the electrolyte with NaCl), the chalcopyrite electrode corrosion current density increases very little as the potential increases, which suggests that another film(s) has formed on the electrode surface and hindereds the electrode dissolution rate. Chalcopyrite is in a pseudo-passive area, which may promote the formation of a pseudo-passive film such as CuS via Reaction (12), according to Nava and Gonzalez [33].

$$2CuFeS_2 + 13H_2O \rightarrow 0.75CuS + 1.25Cu^{2+} + 2Fe^{3+} + 3.25SO_4^{2-} + 26H^+ + 28e^- \quad (12)$$

For the cathodic scan, a notable feature was observed for the solutions with NaCl. Specifically, two negative current peaks were observed between potentials −100 and 30 mV. The negative current peak observed in the anodic polarization region is described as a 'cathodic loop', which is shown in Fig. 2. These 'cathodic loops' are usually observed in studies of metals, and the causes are attributed to oxygen reduction [34] or hydrogen evolution [35]. However, in the present case, oxygen reduction and hydrogen evolution could not be the cause, for the 'cathodic loop'

did not occur for the electrolyte without NaCl. As mentioned above, cupric ions from chalcopyrite could become CuCl and $CuCl_2^-$ for the electrolyte with NaCl, as indicated in Reactions (2) and (3). Thus, the CuCl and $CuCl_2^-$ species formed at the chalcopyrite electrode–electrolyte interface may act as a barrier to the ions entering the solution for which limiting currents were observed at higher potentials. Note that Singh and Ray [36] used this theory to explain the 'cathodic loop'. In order to further confirm the cathodic loops were from copper chloride complexes redox, we used platinum wire electrode substitute chalcopyrite act as the working electrode, and added 5 ml 0.1 mol/L $CuSO_4$ to the electrolytes (30 mL 0.2 mol/L H_2SO_4 with different NaCl concentrations: (a) 0 mol/L; (b) 0.5 mol/L; (c) 1.0 mol/L). Potentiodynamic polarization curves by automatically changing the electrode potential from −160 mV to 230 mV at a scan rate of 0.5 mV s^{-1} are shown as Fig. S1.

According to the above analysis, the electrochemical reactions on the chalcopyrite electrode surface at differential intervals are shown in Table 1.

3.3. Cyclic voltammetry study

Cyclic voltammetry tests of chalcopyrite in 0.2 mol/L sulfuric acid solutions with different NaCl concentrations (0, 0.5, 1.0, 1.25 and 1.5 mol/L) were performed to acquire qualitative information about the electrochemical reactions. In this study, potentiodynamic cycles were performed with a positive-going potential sweep from the OCP to + 0.8 V (for the electrolyte without NaCl)/ 1.0 V (for the electrolyte with NaCl) and back with a negative-going potential sweep from + 0.8 V/1.0 V to − 0.60 V, and then positive-going back to + 0.8 V/1.0 V at a scan rate of 5 mV s^{-1}. The results are shown in Fig. 3.

For the electrolyte with NaCl, the chalcopyrite CV curve (Fig. 3(a)) shows five anodic peaks (A1, A2, A3, A4 and A5) and four cathodic peaks (C1, C2, C3, and C4). When the potential was scanned from the OC potential to + 0.8 V, a $Cu_{1-x}Fe_{1-y}S_2$ surface layer (peaks A1 and A1') was formed, which then transformed into another surface layer (peaks A2 and A2') as the potential increased further. Reactions (5) and (7) are proposed to describe these two electrochemical processes. As the potentials were increased above 0.7 V, the chalcopyrite anodic current density increased dramatically as the scan potential increased, indicating that the electrode enters an active phase. Notably, the potential area corresponds with the potentiodynamic curve results. At this potential area, the entire previous surface layer(s) would be destroyed, giving rise to peak A3, as shown in Reaction (9).

A1: $CuFeS_2 + 4H_2O \rightarrow Cu_{1-x}Fe_{1-y}S_2 + xCu^{2+} + yFe^{3+} + zSO_4^{2-} + 8zH^+ + (2x + 3y + 6z)\,e^-$ (5)

A2: $Cu_{1-x}Fe_{1-y}S_2 \rightarrow Cu_{1-x-z}S_2 + zCu^{2+} + (1-y)Fe^{2+} + 2(z+1-y)\,e^-$ (7)

A3: $CuFeS_2 + 8H_2O \rightarrow Cu^{2+} + Fe^{3+} + 2SO_4^{2-} + 16H^+ + 17e^-$ (9)

Two reduction peaks between 0.4 and − 0.3 V (C1: 0.33 V and C2: − 0.23 V) were evident in the inverse scan. According to Holliday and Richmond [37], these peaks could be attributed to the reduction of Fe^{3+} and Cu^{2+}, as shown in Reactions (13) and (14). Notably, peaks C3 and C4 were observed at potential values between − 0.3 V and − 0.8 V. Arce and Gonzalez [38] and Biegler and Horne [39] attributed these peaks to the reduction of covellite and chalcopyrite, respectively (i.e., Reactions (15) and (16)), whereas Velasquez et al. [40] attributed peak C4 to the reduction of chalcocite according to Reaction (17). The reverse of this reaction accounts for the process associated with anodic peak A4 (from − 0.4 to − 0.3 V).

C1: $Fe^{3+} + e^- \leftrightarrow Fe^{2+}$ (13)

C2: $Cu^{2+} + S^0 + 2e^- \leftrightarrow CuS$ (14)

C3: $CuS + 2H^+ + 2e^- \leftrightarrow Cu_2S + H_2S$ (15)

C4: $2CuFeS_2 + 6H^+ + 2e^- \rightarrow Cu_2S + 2Fe^{2+} + 3H_2S$ (16)

Or: $Cu_2S + 2H_2O + 2e^- \leftrightarrow 2Cu + HS^- + OH^-$ (17)

Peaks A4 and A5 are seldom reported during the dissolution of chalcopyrite in anodic scanning, but they always exist in electrochemical studies of chalcocite and bornite [40,15]. Furthermore, according to the cathodic reaction shown above, peaks A4 (−0.215 V) and A5 (−0.1415 V) are considered by these authors to result from the oxidation of copper (Reaction (18)) and chalcocite (Reaction (19)).

A4: $2Cu + HS^- + OH^- \leftrightarrow Cu_2S + H_2O + 2e^-$ (18)

A5: $Cu_2S \leftrightarrow Cu_{1.92}S + 0.08Cu^{2+} + 0.16e^-$ (19)

The chalcopyrite CV curves for the electrolyte with NaCl (Fig. 3(b–e)) are different than those without NaCl. Peak C1 completely disappears, and the cause may be the fast scan rate (5 mV s^{-1}) causing the disappearance of peak C1. Hence, Cyclic voltammetry tests of chalcopyrite in 0.2 mol/L sulfuric acid

Table 1
Electrochemical reaction on the surface of chalcopyrite electrode in differential intervals (vs. SCE).

Surface condition	Electrolyte	Potential(mV vs. SCE)	Reaction	Ref.
passive	H_2SO_4 (or with Cl^-)	OCP-500	$CuFeS_2 + 4H_2O \rightarrow Cu_{1-x}Fe_{1-y}S_2 + xCu^{2+} + yFe^{3+} + zSO_4^{2-} + 8zH^+ + (2x+3y+6z)e^-$; $CuFeS_2 \rightarrow Cu_{1-x}Fe_{1-y}S_2 + xCu^{2+} + yFe^{2+} + 2(x+y)\,e^-$ $y \gg x$	[27]
Transpassive dissolution/passive	H_2SO_4	500–700	$Cu_{1-x}Fe_{1-y}S_2 \rightarrow Cu_{1-x-z}S_2 + zCu^{2+} + (1-y)Fe^{2+} + 2(z+1-y)\,e^-$	[28]
	H_2SO_4 (with Cl^-)	500–800		
Active	H_2SO_4	700–800	$CuFeS_2 + 8H_2O \rightarrow Cu^{2+} + Fe^{3+} + 2SO_4^{2-} + 16H^+ + 17e^-$	[27,29,30]
	H_2SO_4 (with Cl^-)	800–900	$CuFeS_2 + 3H_2O \rightarrow Cu^{2+} + Fe^{2+} + S_2O_3^{2-} + 6H^+ + 8e^-$; $2S_2O_3^{2-} = S_4O_6^{2-} + 2e^-$	[30–32]
Pseudo-passive	H_2SO_4	>800	$2CuFeS_2 + 13H_2O \rightarrow 0.75CuS + 1.25\ Cu^{2+} + Fe_2(SO_4)_3 + 0.25SO_4^{2-} + 26H^+ + 28e^-$	[33]
			$CuS + 4H_2O \rightarrow Cu^{2+} + SO_4^{2-} + 8H^+ + 8e^-$	[42]
	H_2SO_4 (with Cl^-)	>900	$2CuFeS_2 + 13H_2O \rightarrow 0.75CuS + 1.25\ Cu^{2+} + Fe_2(SO_4)_3 + 0.25SO_4^{2-} + 26H^+ + 28e^-$	[33]
			$2CuS + 11H_2O + Cl^- = Cu_2(OH)_3Cl + 2SO_4^{2-} + 19H^+ + 16e^-$	[42]

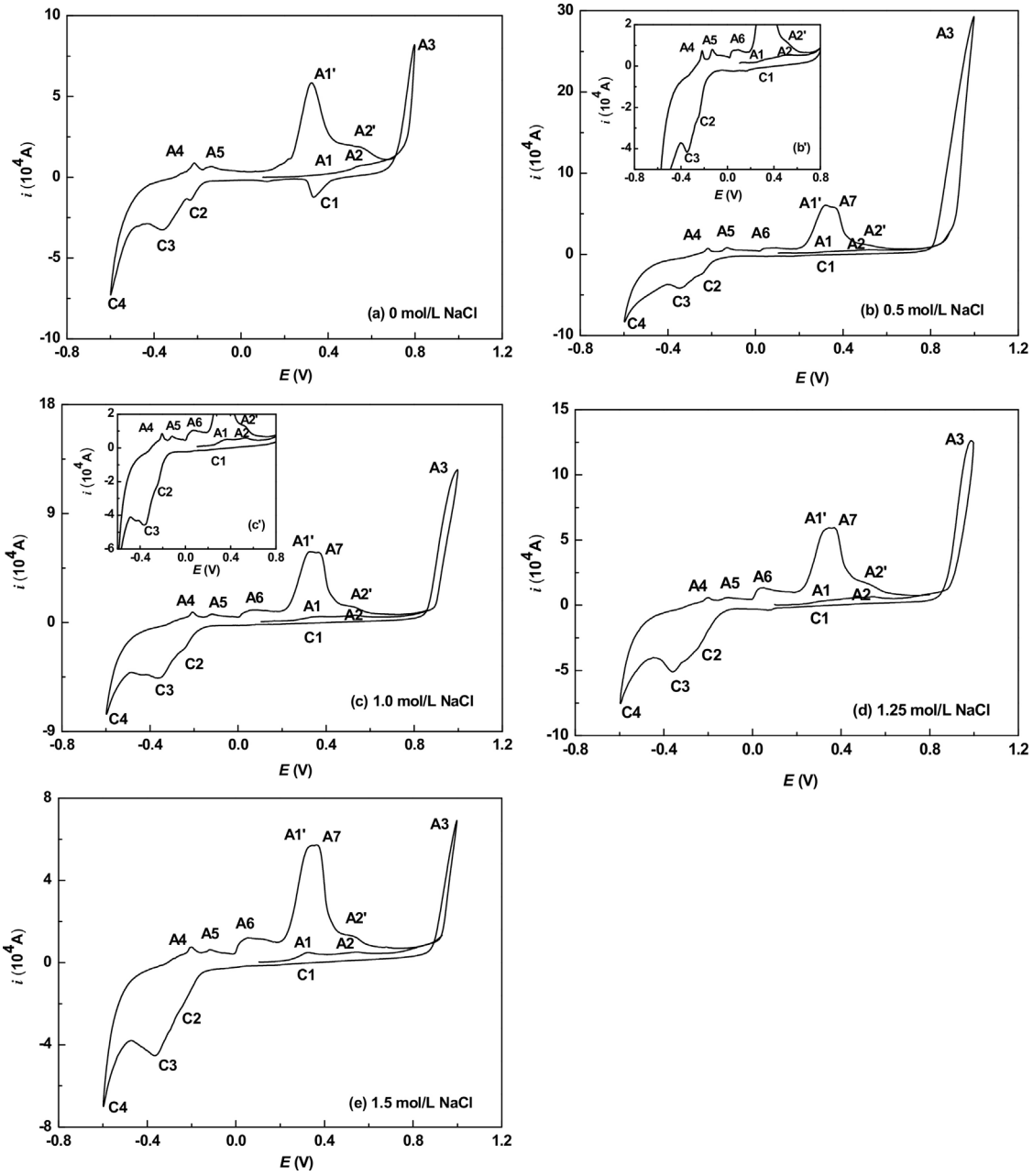

Fig. 3. CV for the chalcopyrite electrode in 0.2 mol/L sulfuric acid with different NaCl concentrations at a scan rate 5 mV S^{-1}.

solutions with different NaCl concentrations (0.5, 1.0, 1.25 and 1.5 mol/L) were further performed and the CV curve is shown in Fig. S2. The Fig. S2 reveals the peak C1 still didn't occur. Howereve, peaks CI and CII were observed at potential values between −100 and 30 mV, which is corresponding with the potentiodynamic results, and these peaks attributed to Cl^- and Cu^{2+} form a series of chloro-complexes. Then, 5 mL 0.1 mol/L Fe^{3+} were added to 30 mL electrolyte (0.2 mol/L H_2SO_4 with different NaCl concentrations: (1) 0.5 mol/L; (2) 1.5 mol/L.) and repeated the CV experiment. The CV curves are shown in Fig. S3 and the peak C1 still didn't occur. According to above experiments and the Fe – Cl – H_2O system analysis, the cause for the peak C1 disappears is Fe^{3+} and Cl^- can complex to two main iron (III) chloride complexes [41]: $Fe^{3+} + Cl^- \rightarrow FeCl_2^{2+}$; $Fe^{3+} + 2Cl^- \rightarrow FeCl_2^{+}$. Senanayake [42] reported under the experimental condition, the iron (III) chloride complexes are stable.

Additionally, two other peaks emerged in the chalcopyrite CV curves during the back anodic scan. One peak occurs near 30 mV (peak A6), which we attribute to CuS from the oxidization of Cu_2S [42–44]; the other peak occurs near 400 mV (peak A7), which we attribute to S from the oxidization of CuS [42–44]. Reactions (20) and (21) show the associated proposed reactions.

$$\text{A6: } Cu_2S + Cl^- = CuCl^+ + CuS + 2e^- \quad (20)$$

$$\text{A7: } CuS + Cl^- = CuCl^+ + S + 2e^- \quad (21)$$

3.4. Electrochemical impedance spectroscopy study

EIS has been widely applied for studying the characteristics of electrodes and electrochemical reactions [45]. In this section, EIS

studies were used to confirm the previous potentiodynamic conclusions and to clarify the electrochemical oxidation mechanism of the chalcopyrite surface in the sulfuric acid solutions at different anodic potentials. Anodic potentials corresponding to different potential regions obtained from the potentiodynamic curves were performed for the EIS experiments. Each potential was applied to the electrode for 400 s to ensure that the steady-state current intensity was reached, which was then followed by EIS measurements. All the EIS data were fitted to equivalent electrochemical circuits (EECs) by a nonlinear method [46]. Since the equivalent circuits represent an approach to describe the electrochemical processes that occur at the electrode/electrolyte interface, any models derived from them are tentative [47]. For this reason, different EECs were used to fit the EIS data, and only those with the best fitted values that could effectively explain the results at the electrode/electrolyte interface were reported.

3.4.1. Passivation area (OCP to 500 mV)

Fig. 4 shows the Nyquist and Bode plots for the chalcopyrite at the OC potential. These results are similar to those obtained by Asswlin et al. [48] and Ghahremaninezhad et al. [26]. The Bode plots in Fig. 4 b) shows that chalcopyrite has two time constants, corresponding to two faradaic relaxation processes at this potential. The first time constant, at high frequencies, is a capacitive loop related to the charge transfer resistance caused by the electrochemical dissolution of the electrode. The second time constant, at middle-low frequencies, is another capacitive loop related to the combination of pseudo-capacitance impedance (caused by the passive layer) and resistance. Clearly, the chalcopyrite phase at high frequencies and modulus decrease for the electrolyte with NaCl. The equivalent circuit shown in Fig. 5(a) was employed to fit the OC potential experimental data. In this model, R_s is the electrolyte and other ohmic resistance to their respective electrochemical circuits and the C_{SC}/R_{SC} pair represents the charge transform capacitive and resistive behavior in the space charge region, respectively. CPE is a constant phase element with resistance R_{CPE} that arises from the electrode roughness [49]. The C_p/R_p pair represents the capacitive and resistive behavior of the passive film on the surface, respectively. The values of the different elements in the equivalent circuit of the OC potential are shown in Table 2. As seen, (1) when the electrolyte NaCl concentration increased from 0 mol/L to 0.5 mol/L, the chalcopyrite electrode charge transfer resistance R_{SC} and surface film resistance R_p dramatically decreased from 4303 $\Omega\,cm^2$ to 708.2 $\Omega\,cm^2$ and from $1.37 \times 10^4\,\Omega\,cm^2$ to $1.26 \times 10^4\,\Omega\,cm^2$, respectively; (2) when the electrolyte NaCl concentration increased from 0.5 mol/L to 1.5 mol/L, the charge transfer resistance R_{SC} decreased from 708.2 $\Omega\,cm^2$ to 89.71 $\Omega\,cm^2$, while the surface film resistance R_p first decreased from $1.26 \times 10^4\,\Omega\,cm^2$ to $9.43 \times 10^3\,\Omega\,cm^2$ and then increased to $2.42 \times 10^4\,\Omega\,cm^2$.

Fig. S4 shows the Nyquist and Bode plots for chalcopyrite at a 400 mV potential. As seen, the plots are similar at the OC potential. Fig. 5(b) depicts the modeled circuit for the 400 mV potential. Compared with the modeled circuit for the OC potential, the Q_p/R_p pair was substituted for the C_p/R_p pair (given the defects in the passive layer [50]) and Q_p was substituted for the capacitor C_p to give a more accurate fit [51]. The values of the different elements in the equivalent 400 mV circuit are shown in Table 3. At this potential: (1) when the electrolyte NaCl concentration increased from 0 mol/L to 0.5 mol/L, the chalcopyrite electrode charge transfer resistance R_{SC} decreased dramatically from 1167 $\Omega\,cm^2$ to 74.89 $\Omega\,cm^2$, while the surface film resistance R_p increased slightly from 3727 $\Omega\,cm^2$ to 6900 $\Omega\,cm^2$; (2) when the NaCl concentration increased from 0.5 mol/L to 1.5 mol/L, the charge transfer resistance R_{SC} decreased from 74.89 $\Omega\,cm^2$ to 20.15 $\Omega\,cm^2$, while the surface film resistance R_p first decreased from 6900 $\Omega\,cm^2$ to 1397 $\Omega\,cm^2$ and then increased to 6253 $\Omega\,cm^2$.

According to the above electrochemical parameters, we can conclude the following for the passive area. At the same potential when the electrolyte changed from not containing NaCl to containing NaCl (in this work 0.5 mol/L), the chalcopyrite electrode charge transfer resistance R_{SC} decreased dramatically, with higher NaCl concentrations leading to smaller R_{SC} values. When the electrolyte had the same NaCl concentration, the chalcopyrite electrode had smaller values of the charge transfer resistance R_{SC} and surface film resistance R_p at higher potentials. The cause of these phenomena is attributed to the ability of chloride ions to adsorb on the surface. This adsorption results in the formation of surface states within the film band gap that aid the passage of current, catalyzing the electrochemical dissolution of the film [52]. Additionally, higher positive potentials result in smaller values of R_{SC} and R_p, revealing that higher positive potentials are beneficial for species across the double layer, and these potentials do not facilitate the accumulation of species on the superficial film.

When the electrolyte NaCl concentration increased from 0 mol/L to 0.5 mol/L, the chalcopyrite electrode surface film resistance R_p decreased dramatically at the OC potential, whereas it increased slightly at 400 mV. Furthermore, as the NaCl concentration increased at these two potentials, the chalcopyrite electrode surface film resistance R_p initially decreased until the NaCl

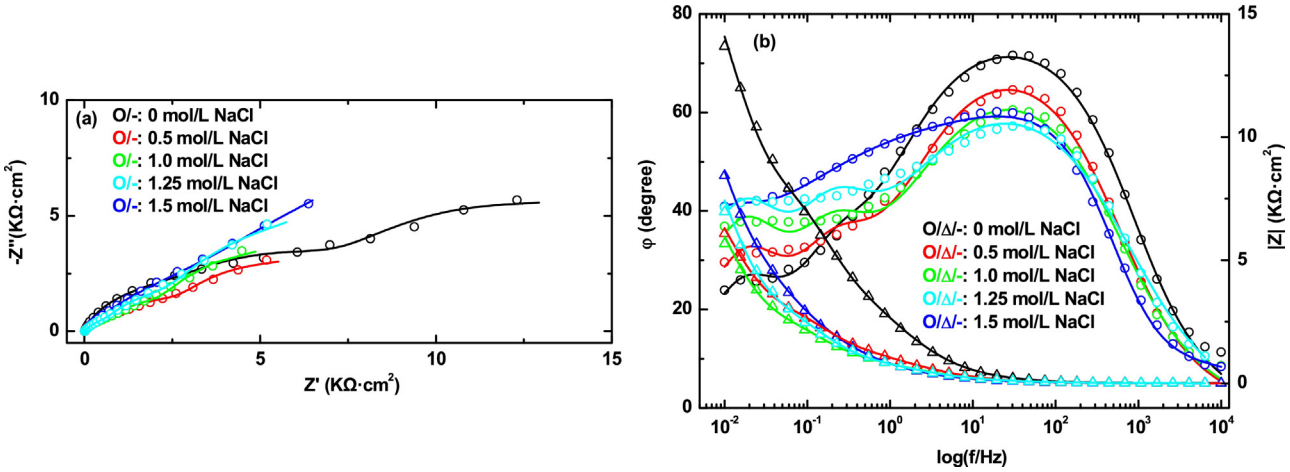

Fig. 4. Nyquist plots (a) and Bode plots (b) of the chalcopyrite electrode in 0.2 mol/L sulfuric acid with different NaCl concentrations at open circuit potential, where (○, Δ) experimental and (–) simulated, (○) angle degree and (Δ) modulus in figure (b).

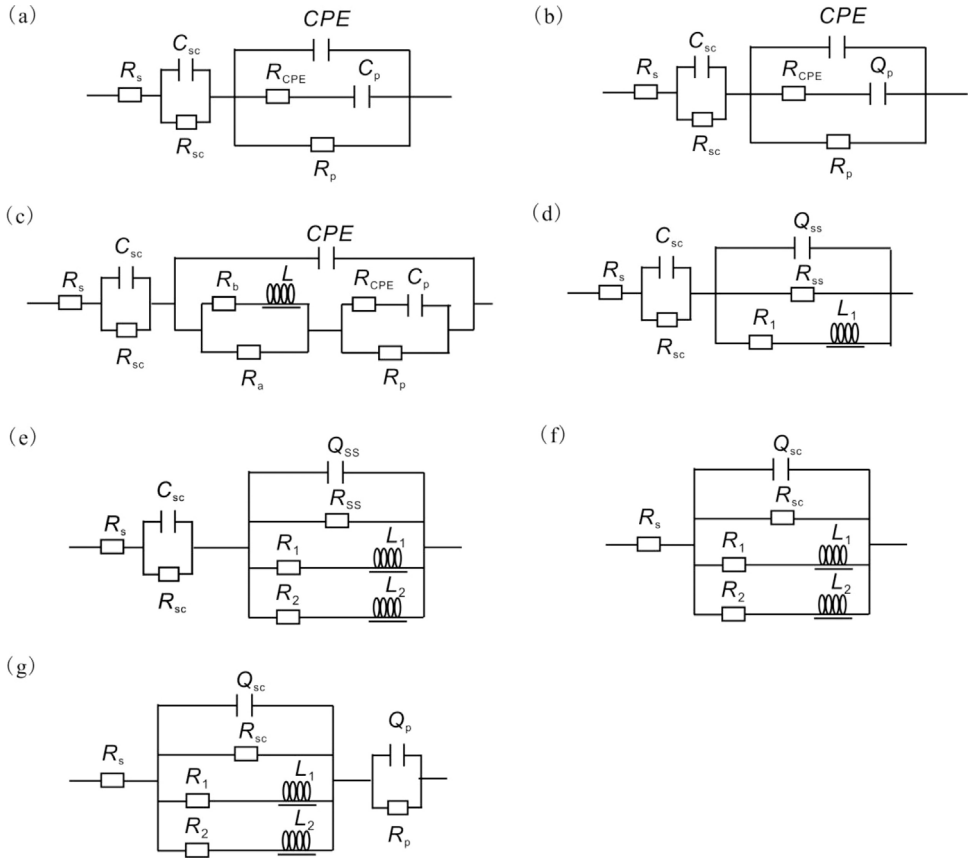

Fig. 5. Equivalent circuits for the chalcopyrite electrode/electrolyte at different anodic potentials.

Table 2
Model parameters for equivalent circuit of Fig. 11(a).

Potential	Electrolyte	R_{sc} (Ω cm^2)	C_{SC} (F cm^{-2})	CPE_1, Y_0 (S cm^{-2} s^{-n})	n	R_{CPE} (Ω cm^2)	C (F cm^{-2})	R_p (Ω cm^2)
OCP	0.2 mol/L H_2SO_4	4303	2.56×10^{-4}	6.13×10^{-5}	0.843	4.60×10^{3}	7.63×10^{-4}	1.37×10^{4}
	0.2 mol/L H_2SO_4, 0.5 mol/L NaCl	708.2	1.48×10^{-5}	1.24×10^{-4}	0.825	2.29×10^{4}	2.12×10^{-4}	1.26×10^{4}
	0.2 mol/L H_2SO_4, 1.0 mol/L NaCl	451.3	1.70×10^{-4}	1.14×10^{-4}	0.800	3.43×10^{4}	1.16×10^{-4}	9.43×10^{3}
	0.2 mol/L H_2SO_4, 1.25 mol/L NaCl	101.3	3.95×10^{-4}	3.49×10^{-4}	0.738	1.16×10^{4}	5.85×10^{-4}	1.84×10^{4}
	0.2 mol/L H_2SO_4, 1.5 mol/L NaCl	89.71	8.72×10^{-4}	1.80×10^{-4}	0.779	1.49×10^{3}	2.05×10^{-3}	2.42×10^{4}

Table 3
Model parameters for equivalent circuit of Fig. 11(b).

Potential (mV)	Electrolyte	R_{sc} (Ω cm^2)	C_{SC} (F cm^{-2})	CPE_1, Y_0 (S cm^{-2} s^{-n})	n	R_{CPE} (Ω cm^2)	CPE_2, Y_0 (S cm^{-2} s^{-n})	n	R_p (Ω cm^2)
400	0.2 mol/L H_2SO_4	1167	6.56×10^{-3}	3.86×10^{-5}	0.857	2136	8.45×10^{-5}	0.522	3727
	0.2 mol/L H_2SO_4, 0.5 mol/L NaCl	74.89	2.90×10^{-5}	2.58×10^{-5}	0.862	913.1	3.30×10^{-4}	0.441	6900
	0.2 mol/L H_2SO_4, 1.0 mol/L NaCl	35.93	3.12×10^{-5}	3.07×10^{-5}	0.839	435.8	5.98×10^{-4}	0.383	1397
	0.2 mol/L H_2SO_4, 1.25 mol/L NaCl	31.26	2.59×10^{-5}	4.32×10^{-5}	0.812	336.1	9.34×10^{-4}	0.399	5839
	0.2 mol/L H_2SO_4, 1.5 mol/L NaCl	20.15	3.43×10^{-5}	3.59×10^{-5}	0.825	285.9	7.35×10^{-4}	0.421	6253

concentration reached 1.0 mol/L and then it increased. This result is likely caused by two opposite actions of Cl^-. On one hand, Cl^- ions can promote electrochemical dissolution of the chalcopyrite electrode. During the previous 400 sec of steady-state progress, this action is advantageous to surface film accumulation. Simultaneously, the Cl^- ions can form CuCl, $CuCl_2^-$ and $CuCl_3^{2-}$, and these cuprous chloride complexes, especially CuCl, can be easily adsorbed on the chalcopyrite anodic electrode surface, thus inhibiting the surface film dissolution. On the other hand, Cl^- ions have a strong tendency to penetrate the surface and can catalyze the electrochemical dissolution of the film, which is advantageous for surface film dissolution. When the NaCl concentration is 0.5 mol/L, Cl^- ions can penetrate and catalyze the surface film dissolution at the OC potential, whereas at 400 mV the added anodic potential is clearly advantageous to the chalcopyrite electrochemical reaction, resulting in a thicker passive surface film. The ability of Cl^- ions to penetrate the surface and catalyze the electrochemical dissolution of the film increases as the NaCl concentration increases, causing a thinner surface film. Meanwhile, an increase in the concentration of Cl^- ions causes the concentration of cuprous chloride complexes to increase, resulting in a thicker surface film. Consequently, these two different actions

of Cl^- ions cause the chalcopyrite electrode passive surface film resistance R_p to initially decrease and then increase as the NaCl concentration increases (to 1.0 mol/L in this work).

3.4.2. Transpassive dissolution/passive area (500–700/800 mV)

According to the results of the potentiodynamic curves, the chalcopyrite electrode moves from the passive area to the transpassive dissolution/passive area as the anodic potential increases. Fig. S5 shows the Nyquist and Bode plots for the chalcopyrite electrode at an anodic potential of 600 mV.

When the electrolyte does not contain chloride ions three time constants are detected in the chalcopyrite Bode plots (Fig. S5 b). The first time constant, at high frequencies, is a capacitive loop related to a combination of the double layer capacitance impedance and charge transfer resistance (caused by the electrochemical dissolution of the electrode). The second time constant, at middle frequencies, is a capacitance related to the combination of pseudo-capacitance impedance (caused by the passive layer, as in Reaction (5)) and resistance. At very low frequencies the Nyquist curve reveals inductive behavior, which is most likely related to the transpassive dissolution of the passive layer according to Reaction (7), and as reported by Bojinov and Tzvetkoff [53]. Based on the above discussion, the equivalent circuit shown in Fig. 5(c) was employed to fit the experimental data, where the C_{SC}/R_{SC} pair represents the charge transform capacitive and resistive behavior in the space charge region, respectively. The parallel connection of $R_a||(LR_b)$ corresponds to the dissolution of the semiconductor electrode, with the impedance consisting of two conductive paths. The first conductive path arises from Reaction (5), which is characterized by resistance R_a in parallel with inductance L, with L corresponding to an intermediate $Cu_{1-x}Fe_{1-y}S_2$ relaxation process. The second conductive path is resistance R_b, which arises from Reaction (7). The R_p/C_p represents the resistance and capacitance of the inner passive film (i.e., directly on the chalcopyrite surface), while *CPE* and R_{CPE} are used to model the outer surface layer. The values of the different elements in the 600 mV equivalent circuit are shown in Table 4. The experimental data show that the chalcopyrite electrode inner passive surface $Cu_{1-x}Fe_{1-y}S_2$ is 2882 $\Omega\,cm^2$ and the outer surface layer $Cu_{1-x-z}S_2$ is 495 $\Omega\,cm^2$. These results are in contrast to the passivation area; for example, the chalcopyrite passivation film resistance of $Cu_{1-x}Fe_{1-y}S_2$ at 400 mV is 3727 $\Omega\,cm^2$. Clearly, the passivation resistance experiences a large decrease, and these data indicate a change from the passivation area to the transpassive dissolution area. Furthermore, the $R_a||(LR_b)$ values are 2.06×10^{-7} $\Omega\,cm^2$, 1.78×10^5 H cm^{-2} and 5.72×10^7 $\Omega\,cm^2$, respectively. Thus, the small R_a value and the large R_b and L values indicate that Reactions (5) and (7) are fast and slow processes, respectively. These results are in agreement with those reported by Hackel et al. [27].

As with the electrolyte without chloride ions, three time constants are detected in the chalcopyrite Bode plots for the electrolyte with chloride ions. One time constant, at high frequencies, is a capacitive loop related to the combination of the double layer capacitance impedance and a charge transfer resistance. A second time constant, at middle frequencies, is a capacitive loop related to the combination of pseudo-capacitance impedance (caused by the passive layer, as in Reaction (6)) and resistance (caused by the electrochemical dissolution of the electrode). The third time constant, at low frequencies, differs from that observed without NaCl; specifically, it is a capacitive loop (as opposed to an inductive loop), and all the Nyquist plots had large variations in the real impedance values around the frequency of 535 mHz. In addition, the magnitude of the value with NaCl is slightly larger than that without NaCl, which suggests that the presence of NaCl is disadvantageous for chalcopyrite transpassive dissolution. Note that this result is consistent with the potentiodynamic curve data. Collectively, these results also indicate that some complexes are likely to be adsorbed on the surface layer and inhibit the transpassive dissolution of chalcopyrite. Furthermore, it is possible to consider that a frequency dependent adsorption (e.g., at 535 mHz) of one of the dissolution products occurs at this point. For example, the cuprous chloride complexes from Reactions (3)–(5) could be good candidates to causes the above phenomena. However, more studies are required to investigate this issue further, as the precise nature of this process remains unknown. Hence, a simple equivalent circuit cannot be used to accurately simulate these Nyquist plots.

Increasing the NaCl concentration from 0.5 mol/L to 1.25 mol/L causes the total impedance of the electrode to decrease by orders of magnitude. Simultaneously, the phase angle diagram of Fig. S5 b shows a decrease in the electrode capacitive behavior at the same NaCl concentration. However, the chalcopyrite in the 1.5 mol/L NaCl solution behaves differently; that is, the magnitude of the total impedance of the electrode in this solution is slightly larger than that in the 1.25 mol/L NaCl solution, and the electrode capacitive behavior is slightly smaller than that in the 1.25 mol/L NaCl solution. These results indicate that increasing the NaCl concentration from 0 mol/L to 1.25 mol/L enhances surface layer dissolution, whereas the surface layer dissolution may be slightly reduced when the NaCl concentration is above 1.25 mol/L. The cause of this phenomenon is attributed to the two different actions of Cl^- ions, as described previously.

3.4.3. Active area (700–800/800–900 mV)

As the pyrite anodic potential continues to increase, the passive layers formed at lower potentials change unsteadily. When the anodic potential increased to 700 mV (for the electrolyte without NaCl) or 800 mV (for the electrolyte with NaCl), none of the passive layers formed at lower potentials were stable and electrochemically active dissolution of the chalcopyrite electrode occurred.

Fig. S6 (a) and Fig. S7 (a) show the Nyquist and Bode plots, respectively, for chalcopyrite at an anodic potential of 750 mV in a 0.2 mol/L H_2SO_4 solution for the electrolyte without NaCl. The high frequency impedance loop is the result of charge transfer resistance and double layer capacitance coupling. The mid-frequency impedance loop and the low frequency inductive impedance loop are characteristic of anodic dissolution of semiconductor electrodes [54]. The equivalent circuit shown in Fig. 5(d) was employed to fit the experimental data, where the C_{SC}/R_{SC} pair represents the charge transform capacitive and the resistive behavior in the space charge region, respectively. The $Q_{ss}||R_1||(L_1R_{SS})$ section of the model represents the dissolution of the semiconductor electrodes, in which Q_{SS} and R_{SS} contribute to the

Table 4
Model parameters for equivalent circuit of Fig. 11 (c).

Potential (mV)	Electrolyte	C_{SC} ($F\,cm^{-2}$)	R_{sc} ($\Omega\,cm^2$)	CPE_1, Y_0 ($S\,cm^{-2}\,s^{-n}$)	n	L ($H\,cm^{-2}$)	R_b ($\Omega\,cm^2$)	R_a ($\Omega\,cm^2$)	C_p ($F\,cm^{-2}$)	R_{cpe} ($\Omega\,cm^2$)	R_p ($\Omega\,cm^2$)
600	0.2 mol/L H_2SO_4	1.10×10^{-3}	292.9	1.12×10^{-4}	0.681	1.78×10^5	5.72×10^7	2.06×10^{-7}	2.49×10^{-6}	2882	495

surface (or interface) states on the electrode, R_1 corresponds to the resistance associated with the accumulation of superficial species and element L_1 is an equivalent inductance that indicates the on-going reaction process. The values of the different elements in the equivalent circuit of 750 mV are shown in Table 5. The data show that when chalcopyrite moves from the transpassive dissolution area to the active dissolution area, the charge transform resistance R_{SC} decreases dramatically from 292.9 $\Omega\,cm^2$ to 35.77 $\Omega\,cm^2$. Additionally, the data show that the electrode has a small accumulation resistance R_1 (56.81 $\Omega\,cm^2$) and a low transfer inductance L_1 (100.9 $H\,cm^{-2}$). Collectively, these data indicate that it is difficult for species to accumulate on the superficial film, and they can easily cross the double layer, behaving as active dissolution species.

Fig. S6 (b–e) and Fig. S6 (b–e) show the Nyquist and Bode plots, respectively, for chalcopyrite at an anodic potential 850 mV for the electrolyte with NaCl. Compared with the plots for the electrolyte without NaCl, these Nyquist and Bode plots show the presence of a new inductive loop and the absence of a capacitive loop in the low frequency region. This result suggests the presence of another product that does not accumulate on the surface. We suggest that this product is formed when $S_2O_3^{2-}$ ions are transformed into $S_4O_6^{2-}$ ions (Reaction (11), $2S_2O_3^{2-} = S_4O_6^{2-} + 2e^-$) over this potential range, as reported by Lehmann et al. [31] and Antonijević et al. [32]. Fig. 5(e) shows the model applied to an 850 mV potential, where the C_{SC}/R_{SC} pair represents the charge transform capacitive and the resistive behavior in the space charge region, respectively. The $C_{ss}||R_{ss}||(L_1R_1)$ section of the model represents the dissolution of the semiconductor electrodes, in which C_{SS} and R_{SS} contribute to the surface (or interface) states on the electrode, R_1 corresponds to the resistance associated with the accumulation of $S_2O_3^{2-}$ ions and element L_1 is an equivalent inductance that corresponds to the $S_2O_3^{2-}$ ion relaxation process. The $L_2||R_2$ section of the model represents the $S_4O_6^{2-}$ ion relaxation process, R_2 corresponds to the resistance associated with the accumulation of $S_4O_6^{2-}$ ions and element L_2 is an equivalent inductance that corresponds to the $S_4O_6^{2-}$ ion relaxation process. The values of the different elements in the equivalent circuit are shown in Table 5. As seen, (1) when the electrolyte contains 0.5 mol/L NaCl, the chalcopyrite has a smaller charge transfer resistance, a smaller $S_2O_3^{2-}$ ion accumulation resistance and a smaller relaxation inductance at a potential of 850 mV compared with the results without NaCl at a potential of 750 mV; (2) when the NaCl concentration increases from 0.5 mol/L to 1.25 mol/L, the chalcopyrite charge transfer resistance decreases from 13.84 $\Omega\,cm^2$ to 3.372 $\Omega\,cm^2$, whereas it increases slightly when the NaCl concentration is above 1.25 mol/L. Furthermore, increasing the NaCl concentration results in a decrease in the dimensionless number n from 1 to 0.918. This result suggests that higher NaCl concentrations increase the roughness of the electrode surface, which benefits chalcopyrite depletion. In summary, the above data show that the electrochemical dissolution of chalcopyrite benefits from increasing NaCl concentrations between 0 ~ 1.25 mol/L. In contrast, NaCl concentrations above 1.25 mol/L may slightly inhibit its electrochemical dissolution; and (3) the magnitudes and phases of the chalcopyrite Bode plots all increase as the NaCl concentration increases. Apparently, increasing the NaCl concentration does not benefit the electrochemical dissolution of chalcopyrite in this active dissolution area. Specifically, when the NaCl concentration increases from 0.5 mol/L to 1.5 mol/L, the values of the $L_1||R_1$ parameters increases from 1.42 $H\,cm^{-2}$ to 2105 $H\,cm^{-2}$ and from 33.15 $\Omega\,cm^2$ to 1.24×10^4 $\Omega\,cm^2$, respectively, and the values of the $L_2||R_2$ parameters increase from 47.85 $H\,cm^{-2}$ to 4.56×10^4 $H\,cm^{-2}$ and from 4.172 $\Omega\,cm^2$ to 1305 $\Omega\,cm^2$, respectively. The relatively small value of L_1 and the relatively large value of R_1 indicate that chalcopyrite is easily oxidized to $S_2O_3^{2-}$ ions. In contrast, the relatively large value of L_2 and the relatively small value of R_2 indicate that the oxidation of $S_2O_3^{2-}$ to $S_4O_6^{2-}$ is a more difficult process at this potential. Overall, the above results show two different actions of chloride ions. On one hand, chloride ions initiate the electrochemical dissolution of chalcopyrite because of its strong penetrability, which is evident from the C_{SC}/R_{SC} results. On the other hand, the chloride and cupric ions generated from the oxidation of chalcopyrite can form cuprous complexes such as $CuCl^0$, $CuCl_2^-$ or $CuCl_3^{2-}$, and the presence of these cuprous chloride complexes dramatically inhibits the on-going dissolution of chalcopyrite, which is reflected in the increase of the L_1, R_1, L_2 and R_2 values as the NaCl concentration increases.

3.4.4. Pseudo-passivation area (>800 mV/900 mV)

The previous potentiodynamic curves showed that chalcopyrite from an active area moved to a pseudo-passive area when the anodic potential was above 800 mV (electrolyte without NaCl) or above 900 mV (electrolyte with NaCl). Fig. S8 (a–e) and Fig. S9 (a–e) show the Nyquist and Bode plots for the chalcopyrite electrode in 0.2 mol/L H_2SO_4 solutions with different NaCl concentrations at an anodic potential of 1000 mV.

Similar features are observed for the Nyquist and Bode plots of the chalcopyrite in 0.2 mol/L H_2SO_4 solutions at NaCl concentrations of 0 mol/L and 0.5 mol/L, as shown in Fig. S8 (a, b) and Fig. S9 (a, b), respectively. That is, an impedance loop shows that coupling occurs between the charge transfer resistances and double layer capacitance at high frequency. At middle frequency, an inductive loop represents the anodic dissolution of the semiconductor electrode, and another inductive loop is present at low frequency. Note that an impedance loop does not return to the first quadrant, which corresponds to a pseudo-passive characteristic, as shown in the potentiodynamic curve, indicating that another anodic reaction may be operative. To this end, we deduce the presence of a pseudo-passive film CuS, in accordance with the results from the potentiodynamic curve (Reaction (12)). However, it is possible that further activation of CuS occurred during the 400 s steady-state process. The cause(s) of this possible result includes: (1) the pseudo-passive film CuS was oxidized to Cu^{2+} and SO_4^{2-} in the 0.2 mol/L H_2SO_4 electrolyte solution, as shown in Reaction (22) and reported by Nava and Gonzalez [33]; (2) Cl^- caused a further activation of CuS when the electrolyte contained 0.5 mol/L NaCl in the 0.2 mol/L H_2SO_4 solution. Miki and Nicol [55] reported linear sweep voltammograms of synthetic covellite (CuS) in a mixed H_2SO_4/NaCl system, which showed that

Table 5
Model parameters for equivalent circuit of Fig. 11 (d) and (e).

Potential (mV)	Electrolyte	R_{sc} ($\Omega\,cm^2$)	C_{SC} ($F\,cm^{-2}$)	CPE_1, Y_0 ($S\,cm^{-2}\,s^{-n}$)	n	R_{ss} ($\Omega\,cm^2$)	L_1 ($H\,cm^{-2}$)	R_1 ($\Omega\,cm^2$)	L_2 ($H\,cm^{-2}$)	R_2 ($\Omega\,cm^2$)
750	0.2 mol/L H_2SO_4	35.77	3.83×10^{-6}	6.08×10^{-6}	0.978	63.64	100.9	56.81		
850	0.2 mol/L H_2SO_4, 0.5 mol/L NaCl	13.84	2.08×10^{-7}	2.99×10^{-6}	1.000	26.91	1.42	33.15	47.98	4.17
	0.2 mol/L H_2SO_4, 1.0 mol/L NaCl	4.24	2.74×10^{-6}	4.44×10^{-4}	0.929	303	30.75	290.9	1.32×10^3	31.5
	0.2 mol/L H_2SO_4, 1.25 mol/L NaCl	3.37	2.59×10^{-6}	4.30×10^{-6}	0.922	1238	578.4	1.92×10^3	1.41×10^4	205.8
	0.2 mol/L H_2SO_4, 1.5 mol/L NaCl	7.40	3.90×10^{-7}	4.66×10^{-6}	0.918	3406	2105	1.24×10^4	4.56×10^4	1305

active dissolution at low potentials was followed by passivation at approximately 0.6 V (SHE). According to the results of their potential-pH diagram, Senanayake [44] predicted the dissolution of CuS to form $CuCl^+$ via Reaction (21). According to the above analysis, Fig. 5(f) was employed to fit the Nyquist and Bode plots of chalcopyrite in a 0.2 mol/L H_2SO_4 solution with a NaCl concentration of 0 mol/L and 0.5 mol/L. In this model, Q_{sc}, R_{sc}, R_1/L_1 and R_2/L_2 are in a parallel system, and the double layer may be very thin at this high anodic potential, which leads to better fitted values by this EEC. The values of the different elements in the equivalent circuit are shown in Table 6. As seen, (1) for the electrolyte in a 0.2 mol/L H_2SO_4 solution, the relatively large value of L_1 (41.8 H cm^{-2}) and the relatively small value of R_2 (3.114 Ω cm^2) indicate that the oxidation of chalcopyrite to CuS may be difficult at this potential. In contrast, the relatively small value of L_1 (1.53 H cm^{-2}) and the relatively large value of R_1 (21.6 Ω cm^2) indicate that the oxidation of CuS to Cu^{2+} ions occurs easily under these conditions; (2) when the electrolyte contained 0.5 mol/L NaCl in the 0.2 mol/L H_2SO_4 solution, the relatively small values of L_1 (0.486 H cm^{-2}) and R_1 (1.288 Ω cm^2) indicate that chalcopyrite can be easily oxidized to $S_2O_3^{2-}$ ions. In contrast, the relatively large values of L_2 (36.9 H cm^{-2}) and R_2 (7.375 Ω cm^2), which differs from chalcopyrite in the active area with 0.5 mol/L NaCl, indicate that the oxidation of $S_2O_3^{2-}$ to $S_4O_6^{2-}$ is a more difficult process, revealing that CuCl affects the inductive and resistance behaviors of the system.

The chalcopyrite Nyquist plots (Fig. S8 (c–e)) and Bode plots (Fig. S9 (c–e)) show the presence of three time constants when the electrolyte contains 1.0 mol/L, 1.25 mol/L and 1.5 mol/L NaCl. The first time constant, at high frequencies, is a capacitive loop related to the combination of the double layer capacitance impedance and charge transfer resistance (caused by the electrochemical dissolution). The second time constant, at middle frequencies, is a distorted inductive loop related to a new anodic reaction and transfer process. The third time constant, at very low frequencies, is an impedance loop (caused by the passive surface). In contrast to the results for NaCl solutions with concentrations of 0 mol/L and 0.5 mol/L NaCl, a passive film is truly present in this case. To understand the cause of this phenomenon, we refer to Senanayake [42], who predicted the dissolution of CuS to $CuCl^+$ via Reaction (21) and the passivation caused by the formation of insoluble $Cu_2(OH)_3Cl$ via Reaction (23). Note that the reaction occurs more readily when there is inadequate mass transfer to the liquid phase, causing an oxygen deficiency [43]. Clearly, the high NaCl concentration of the electrolyte causes oxygen deficiency in this work. Fig. 5(g) shows the model applied to simulate the Nyquist plots presented in Fig. S8 (c–e). In this model, the circuit components Q_p and R_p represent the formation and associated properties of the surface layer on the electrode, with the physical interpretation of the other circuit components being similar to Fig. 5(f). The values of the different elements in the equivalent circuit are shown in Table 6. As seen, when the NaCl concentration increased from 1.0 mol/L to 1.5 mol/L at an anodic potential of 1000 mV, the chalcopyrite electrode surface layer resistance R_p decreased from 5.056 Ω cm^2 to 1.389 Ω cm^2 and then increased to 2.494 Ω cm^2, which we can compare to the results for the passive area, where the value of the surface layer resistance ranged from the thousands to the tens of thousands. Here, the R_p values are very small, which is consistent with its pseudo-passive characteristics. Furthermore, the chalcopyrite charge transfer resistance R_{SC} decreased from 6.758 Ω cm^2 to 6.735 Ω cm^2 and then increased to 17.41 Ω cm^2 when the NaCl concentration increased from 0 mol/L to 1.5 mol/L. Overall, the experimental results indicate that a high concentration of chloride ions is disadvantageous for chalcopyrite dissolution.

$$CuS + 4H_2O \rightarrow Cu^{2+} + SO_4^{2-} + 8H^+ + 8e^- \quad (22)$$

$$2CuS + 11H_2O + Cl^- = Cu_2(OH)_3Cl + 2SO_4^{2-} + 19H^+ + 16e^- \quad (23)$$

4. Conclusions

The present study considered the electrochemical dissolution of chalcopyrite in 0.2 M sulfuric acid solutions with different concentrations of sodium chloride. The OCP experiments showed that the chalcopyrite open circuit potential (approximately 245 mV vs. SCE) decreased as the NaCl concentration increased, which was caused by the formation of cuprous complexes such as $CuCl^0$, $CuCl_2^-$ or $CuCl_3^{2-}$ and limited oxygen dissolution. Potentiodynamic polarization revealed four different chalcopyrite surface conditions at different anodic potentials. The first passive area formed a $Cu_{1-x}Fe_{1-y}S_2$ passive layer (OCP–500 mV vs. SCE) via Reaction (5) and/or (6); a second passive layer ($Cu_{1-x-z}S_2$) then formed via Reaction (7) at the transpassive dissolution/passive area (500–700 mV for the electrolyte without NaCl and 500–800 mV with NaCl); and the third area occurred at 700–800 mV (electrolyte without NaCl) or 700–800 mV (electrolyte with NaCl) and involved the disappearance of the passive layer and chalcopyrite in the active area. Notably, a different result is obtained for the electrolyte without NaCl; specifically, the oxidation of sulphide sulphur generated SO_4^{2-} in this electrolyte, whereas $S_2O_3^{2-}$ and $S_4O_6^{2-}$ were formed following the oxidation of sulphide sulphur with the electrolyte with NaCl. In the pseudo-passive area (above 800 mV without NaCl or above 900 mV with NaCl), a CuS film formed via Reaction (12). The observations of the present study were explained based on the results of previously published reports. Cyclic voltammetry experiments provided qualitative information on the electrochemical reactions. The results from these experiments supported the potentiodynamic results and revealed that the oxidation of chalcopyrite produced Cu_2S and CuS, which could be further oxidized by Cl^- ions via Reactions (20) and (21). Finally, EIS was used to support the proposed sequence of chalcopyrite dissolution and surface layer

Table 6
Model parameters for equivalent circuit of Fig. 11 (f) and (g).

Potential (mV)	Electrolyte	CPE_1, Y_0 ($S\,cm^{-2}\,s^{-n}$)	n	R_{sc} (Ω cm^2)	L_1 (H cm^{-2})	R_1 (Ω cm^2)	L_2 (H cm^{-2})	R_2 (Ω cm^2)	CPE_2, Y_0 ($S\,cm^{-2}\,s^{-n}$)	n	R_p (Ω cm^2)
1000	0.2 M H_2SO_4	2.96×10^{-5}	0.800	6.76	41.80	3.11	1.53	21.6	–	–	–
	0.2 M H_2SO_4, 0.5 M NaCl	6.30×10^{-6}	0.914	6.74	0.49	1.29	36.90	7.38	–	–	–
	0.2 M H_2SO_4, 1.0 M NaCl	4.78×10^{-6}	0.922	9.54	19.86	1.0×10^{-6}	1.03	10.42	0.52	0.800	5.06
	0.2 M H_2SO_4, 1.25 M NaCl	4.80×10^{-6}	0.925	14.55	2.26	39.87	5.22	11.39	0.53	0.800	1.39
	0.2 M H_2SO_4, 1.5 M NaCl	5.02×10^{-6}	0.896	17.41	2.45	35.53	8.80	10.07	1.70	1.000	2.49

formation. Different EECs were modeled, and the experimental results revealed that Cl^- ions are advantageous for chalcopyrite dissolution. However, the formation of chloride and cupric ions via the oxidation of chalcopyrite could form the cuprous complexes $CuCl^0$, $CuCl_2^-$ or $CuCl_3^{2-}$, which could dramatically inhibit the ongoing dissolution of chalcopyrite. Thus, high concentrations of Cl^- ions were not essential for chalcopyrite dissolution under the present conditions. Finally, chalcopyrite experienced different electrochemical mechanisms at the four potential areas examined, resulting in specific Cl^- ion concentrations in these areas, namely, 1.0 mol/L in the passive area; 1.25 mol/L in the transfer-passive area; 1.25 mol/L in the active area and 0.5 mol/L in the pseudo-passive area.

Acknowledgments

This work was supported by a CSIRO (Australia) OCE Science Leader Grant, China Scholarship Council, NSFC (40803017) and Key Technologies R & D Program, Guizhou (SY[2011]3088).

Appendix A. Supplementary data

Supplementary data associated with this article can be found, in the online version, at http://dx.doi.org/10.1016/j.electacta.2017.09.063.

References

[1] M.J. Nicol, 1984. The Electrochemical Society, Pennington, NJ, 1984, p. 152.
[2] R.I. Holliday, W.R. Richmond, J. Electroanal. Chem. 288 (1990) 83.
[3] G. Chen, H.Y. Yang, Int. J. Electrochem. Sci. 11 (2016) 34.
[4] A. Ghahremaninezhad, D.G. Dixon, E. Asselin, Electrochim. Acta. 87 (2013) 97–112.
[5] G. Yue, E. Asselin, Electrochim. Acta. 146 (2014) 307.
[6] C.A.C. Sequeira, D.M.F. Santos, J. Appl. Electrochem. 40 (2010) 123.
[7] O.G. Olvera, L. Quiroz, D.G. Dixon, E. Asselin, Electrochim. Acta. 127 (2014) 7.
[8] M. Ammou-Chokroum, P.K. Sen, F. Fouques, Mem. Sci. Revue Metallurgie 76 (1979) 333.
[9] M. Ammou-Chokroum, P.K. Sen, F. Fouques, Proc. XIII Intern Mineral Proc. Cong., Warsaw, Poland, 1979, pp. 527.
[10] R.S. McMillan, D.J. MacKinnon, J.E. Dutrizac, J. Appl. Electrochem. 6 (1982) 743.
[11] C.L. Aguirre, N. Toro, N. Carvajal, H. Watling, C. Aguirre, Miner, Engineer 99 (2016) 60.
[12] M.J. Nicol, S.C. Zhang, Hydrometall. 166 (2016) 167.
[13] H.R. Watling, Hydrometall. 146 (2014) 96.
[14] M.C. Ruiz, K.S. Montes, R. Padilla, Hydrometall. 109 (2011) 37.
[15] Z.Y. Lu, M.I. Jeffrey, F. Lawson, Hydrometallurgy 56 (2000) 189.
[16] T. Havlík, R. Kammel, Miner. Eng. 10 (1995) 1125.
[17] F. Lawson, C.Y. Chen, L.S.Y. Lee, Miner. Process. Extr. Metall. Rev. 8 (1992) 183.
[18] Z.Y. Lu, F. Lawson, Proceedings of the Third International Conference on Hydrometallurgy, International Academic Publishers, Beijing, 1998, pp. 191.
[19] B.R. Palmer, C.O. Nebo, M.F. Rau, M.C. Fuerstenau, Met. Trans. B 12 (1981) 595.
[20] M.M. Antonijevíc, R. Mihajlovíc, B. Vukanovíc, J. Serb. Chem. Soc. 59 (1994) 329.
[21] H. Moslemi, P. Shamsi, F. Habashi, Miner. Engineer. 24 (2011) 1038.
[22] D.L. Jones, E. Peters, The leaching of chalcopyrite with ferric sulphate and ferric chloride, in: J.C. Yannopoulos, J.C. Agarwaal (Eds.), Extractive Metallurgy of Copper, AIME, New York, 1976, pp. 633.
[23] J.D. Miller, P.J. McDonough, H.Q. Portillo, Electrochemical model in silver catalysed ferric sulfate leaching of chalcopyrite, in: J. Laskowski (Ed.), 13th International Mineral Processing Congress, Elsevier, Amsterdam, 1981, pp. 851.
[24] H.K. Lin, X.J. Wu, P.D. Rao, JOM 43 (1991) 60.
[25] M. Lundström, Chalcopyrite dissolution in cupric chloride solutions. Doctoral Thesis, Helsinki University of Technology, FIN-02015 TKK, Finland, 2009.
[26] A. Ghahremaninezhad, E. Asselin, D.G. Dixon, Electrochim. Acta 55 (2010) 5041.
[27] R.P. Hackl, D.B. Dreisinger, E. Peters, J.A. King, Hydrometall. 39 (1995) 25.
[28] A.J. Parker, R.L. Paul, G.P. Power, J. Electroanal. Chem. 118 (1981) 305.
[29] T. Biegler, J. Electrochem. Soc. 85 (1977) 101.
[30] I. Lazaro, M.J. Nicol, J. Appl. Electrochem. 36 (2006) 425.
[31] M.N. Lehmann, M. Stichnoth, D. Walton, S.I. Bailey, J. Electrochem. Soc. 147 (2000) 3263.
[32] M.M. Antonijević, M.D. Dimitrijević, S.M. Šerbula, V.L.J. Dimitrijević, G.D. Bogdanović, S.M. Milić, Electrochim. Acta 50 (2005) 4160.
[33] D. Nava, I. Gonzalez, Electrochim. Acta 51 (2006) 5295.
[34] J.W. Lee, K. Osseo-Asare, H.W. Pickering, J. Electrochem. Soc. 132 (1985) 550.
[35] R.P. Frankenthal, J. Electrochem. Soc. 114 (1967) 542.
[36] V.B. Singh, M. Ray. J. Mater. Sci. 42 (2007) 8279.
[37] R.I. Holliday, W.R. Richmond, J. Electroanal. Chem. 288 (1990) 83.
[38] E.M. Arce, I. Gonzalez, Int. J. Miner. Proce. 67 (2002) 17.
[39] T. Biegler, M.D. Horne, J. Electrochem. Soc. 132 (1985) 1363.
[40] P. Velasquez, D. Leinen, J. Pascual, J.R. Ramos-Barrado, R. Cordova, H. Gomez, R. Schrebler, J. Electroanal. Chem. 510 (2001) 20.
[41] D.K. Nordstrom, L.N. Plummer, D. Langmuir, E. Busenberg, H.M. May, B.F. Jones, Revised chemical equilibrium data for major water–mineral reactions and their limitations, in: D.C. Melchior, R.L. Bassett (Eds.), Chemical modeling of aqueous systems II, American Chemical Society, Washington, DC, 1990.
[42] G. Senanayake, Hydrometallurgy 98 (2009) 21.
[43] H. Miki, M. Nicol, Synergism in the oxidation of covellite and pyrite by iron(III) and copper(II) ions in chloride solutions, Hydrometallurgy 2008: 6th International Symposium (2008) p. 17.
[44] C.Y. Cheng, F. Lawson. Hydrometallurgy 27 (1991) 249.
[45] M. Orazem, B. Tribollet, Electrochemical Impedance spectroscopy, Second ed., John Wiley and Sons, New Jersey, 2008, pp. 38.
[46] B.A. Boukamp, Solid State Ionics 26 (1986) 31.
[47] J.R. Macdonald, J. Appl. Phys. 58 (1985) 1971.
[48] E. Asselin, A. Alfantazi, S. Rogak, J. Electrochem. Soc. 154 (2007) C215.
[49] W.H. Mulder, J.H. Sluyters, T. Pajkossy, L. Nyikos, J. Electroanal. Chem. 285 (1990) 103.
[50] L. Chen, Y. Zhou, S. Krause, A.G. Munoz, J. Kunze, P. Schmuki, Electrochim. Acta. 53 (2008) 3395.
[51] J.E. Ferrer, L.L. Victori, Electrochim. Acta. 39 (1994) 581.
[52] F.K. Crundwell, Hydrometallurgy 21 (1988) 155.
[53] M. Bojinov, T. Tzvetkoff, J. Phys. Chem. B 21 (2003) 5101.
[54] W.P. Gomes, D. Vanmaekelbergh, Electrochim. Acta. 41 (1996) 967.
[55] H. Miki, M.J. Nicol, Synergism in the oxidation of covellite and pyrite by iron (III) and copper (II) ions in chloride solutions, in: C.A. Young, P.R. Taylor, C.G. Anderson, Y. Choi (Eds.), Hydrometallurgy Proc. 6th International Symposium, SME Littleton, 2008, pp. 646.